doi:10.1038/nature18284

Lanthanum-catalysed synthesis of microporous 3D graphene-like carbons in a zeolite template

Kyoungsoo Kim[1], Taekyoung Lee[1,2], Yonghyun Kwon[1,2], Yongbeom Seo[1], Jongchan Song[3], Jung Ki Park[3], Hyunsoo Lee[1], Jeong Young Park[1,4], Hyotcherl Ihee[1,2], Sung June Cho[5] & Ryong Ryoo[1,2]

Three-dimensional graphene architectures with periodic nanopores—reminiscent of zeolite frameworks—are of topical interest because of the possibility of combining the characteristics of graphene with a three-dimensional porous structure[1–6]. Lately, the synthesis of such carbons has been approached by using zeolites as templates and small hydrocarbon molecules that can enter the narrow pore apertures[7–15]. However, pyrolytic carbonization of the hydrocarbons (a necessary step in generating pure carbon) requires high temperatures and results in non-selective carbon deposition outside the pores. Here, we demonstrate that lanthanum ions embedded in zeolite pores can lower the temperature required for the carbonization of ethylene or acetylene. In this way, a graphene-like carbon structure can be selectively formed inside the zeolite template, without carbon being deposited at the external surfaces. X-ray diffraction data from zeolite single crystals after carbonization indicate that electron densities corresponding to carbon atoms are generated along the walls of the zeolite pores. After the zeolite template is removed, the carbon framework exhibits an electrical conductivity that is two orders of magnitude higher than that of amorphous mesoporous carbon. Lanthanum catalysis allows a carbon framework to form in zeolite pores with diameters of less than 1 nanometre; as such, microporous carbon nanostructures can be reproduced with various topologies corresponding to different zeolite pore sizes and shapes. We demonstrate carbon synthesis for large-pore zeolites (FAU, EMT and beta), a one-dimensional medium-pore zeolite (LTL), and even small-pore zeolites (MFI and LTA). The catalytic effect is a common feature of lanthanum, yttrium and calcium, which are all carbide-forming metal elements. We also show that the synthesis can be readily scaled up, which will be important for practical applications such as the production of lithium-ion batteries and zeolite-like catalyst supports.

Zeolites are a family of microporous crystalline aluminosilicate materials, which fall into more than 200 structural types[16]. Each structural type is distinguished by its unique pore structure—for example, in terms of its pore diameters, shapes and connectivity[17]. The pore diameters are typically between 0.3 nm and 1.3 nm. Another important characteristic of zeolites is their ion-exchange capacity[18,19]. Zeolite frameworks contain cations to compensate for the negative charge at the aluminiums in the tetrahedral silicate framework. The cations—which, as synthesized, are normally sodium or ammonium ions—can be exchanged with other cations through a solution-based conventional ion-exchange process.

In recent years, zeolites have attracted attention as a template for carbon synthesis[7–15,20,21]. The pores in many zeolites have diameters appropriate to accommodating fullerene and carbon nanotubes, and are interconnected along the smoothly curved surface to form a three-dimensional (3D) network that is open to the exterior. In principle, such a nanoporous system should be ideal as a template for synthesizing a 3D graphene architecture[8–11]. However, the zeolite pores are too small to accommodate bulky molecular compounds, such as sucrose, polyaromatic compounds, and furfuryl alcohol, which are commonly used for carbon synthesis with mesoporous silica templates[20,21]. Small molecules, such as ethylene and acetylene, are desirable as a carbon source for achieving successful carbonization within the zeolite pores. But carbonization of these small hydrocarbons generally requires high-temperature reactions to fix the carbon source inside the pores. At such high temperatures, the reactions tend to occur non-selectively on the external surfaces as well as on the internal pore walls[13–15]. This often results in coke being deposited at the external surfaces, causing serious diffusion limitations into the pores.

Here we tackled this problem by using La^{3+} ions. We intuited that such a transition-metal element would bond with olefins, acetylenes and aromatic compounds through a d–π coordination. If so, then the d–π interactions should stabilize ethylene and the pyrocondensation intermediates to form a carbon framework in zeolite. Then, we would expect carbonization to occur selectively inside the La^{3+}-containing zeolite pores.

To test this hypothesis, we carried out ion exchange of an Na^+-containing form of the zeolite faujasite-Y (FAU-Y; that is, NaY zeolite) with La^{3+}. We heated the resulting LaY zeolite under carbon-synthesis conditions using ethylene gas for 1 hour at different temperatures (see Methods). We analysed the amount of carbon deposition at each temperature by thermogravimetry, and plotted the analysis data as a function of temperature (Extended Data Fig. 1). We also compared these LaY data with the results obtained from other cation-containing forms of the zeolite, such as NaY and HY. The data indicate that the LaY, NaY and HY zeolite samples all show rapid carbon deposition at 800 °C. However, as the temperature decreases, the different ionic forms behave dramatically differently: at 600 °C, the LaY zeolite is still active as a carbon-deposition template, whereas both NaY and HY lose this function almost completely. This result highlights a catalytic effect of lanthanum on carbonization. Usually, in carbon synthesis, the proton form of zeolite is preferred as a template. This is due to the presence of Lewis and Brønsted acid sites that can catalyse the pyrocondensation of hydrocarbons into polymeric coke species[22]. But carbon deposition in LaY occurs more than 20 times faster than in such an acidic HY zeolite (based on our chosen ethylene flow for 1 hour at 600 °C). The ethylene flow can also be safely prolonged until all internal pores are fully saturated with carbon; the deposition of any amorphous or graphitic carbon on external surfaces is still prevented (Extended Data Fig. 2).

We investigated the carbon structure using solid-state, magic-angle spinning ^{13}C nuclear magnetic resonance (NMR) spectroscopy after the deposition of ^{13}C-labelled carbon in the LaY zeolite

---

[1]Center for Nanomaterials and Chemical Reactions, Institute for Basic Science (IBS), Daejeon 305-701, Korea. [2]Department of Chemistry, KAIST, Daejeon 34141, Korea. [3]Department of Chemical and Biomolecular Engineering, KAIST, Daejeon 34141, Korea. [4]Graduate School of EEWS, KAIST, Daejeon 34141, Korea. [5]Clean Energy Technology Laboratory and Department of Chemical Engineering, Chonnam National University, Gwangju 61186, Korea.

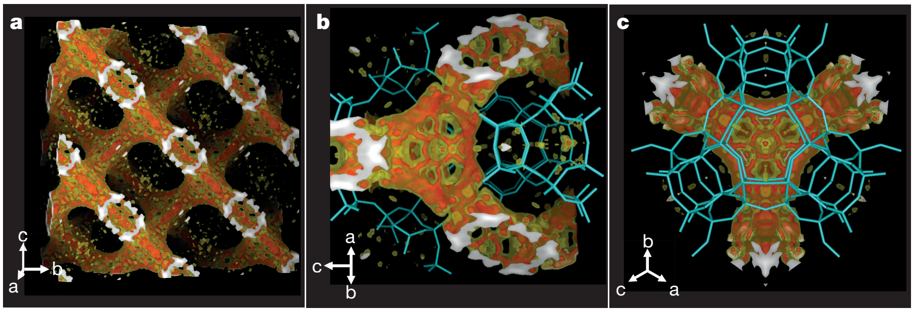

Figure 1 | Electron-density map of the supercage of zeolite FAU after carbon deposition. a, Three-dimensional electron-density map of the carbon framework formed at 600 °C, excluding the zeolite framework. **b**, **c**, Enlarged images of the electron-density map, including the zeolite framework (cyan), from different viewpoints: along the (110) axis (**b**) and the (111) axis (**c**). The electron-density map corresponds to the electron-density difference between zeolite and the carbon–zeolite composite, and was obtained using the difference Fourier method. The iso-surface level of the electron density is set to 0.25 electrons per Å^3 (yellow) and 0.35 electrons per Å^3 (red). White areas represent cross-sectional cuts.

(Extended Data Fig. 3). The NMR spectrum exhibits two slightly separated peaks (at 123 and 129 parts per million, p.p.m.). These NMR peaks can be interpreted as sp^2 carbon species in six-membered, and in five- or seven-membered, carbon rings respectively[23]. Thus, all carbon atoms in the zeolite–carbon composite sample have an sp^2 hybridized bonding nature within the detection limit of the ^{13}C NMR spectroscopy.

Here, the question is whether the carbon structure is built systematically like a 3D graphene along smoothly curved surfaces on pore walls, or exists randomly in the template pore volume. We sought the answer by studying X-ray diffraction (XRD) data of large single crystals of FAU after carbon deposition. Figure 1a shows an electron-density map of atoms that were brought into the zeolite micropore (designated the 'supercage') during carbon deposition. We obtained this map by using the difference Fourier method with X-ray single-crystal diffraction data, which we collected after fully dehydrating the zeolite–carbon composite sample (to exclude moisture in the supercage) by flowing nitrogen gas at 600 °C and then placing the sample in a vacuum at 350 °C (see Methods). All of the electron densities in the supercage can thus be attributed to carbonaceous frameworks.

The electron densities indicate diffused atomic positions in the wide section of the supercage; these atomic positions correspond to a hexagonal ring of carbon atoms, as in a graphene net (Fig. 1b, c). In particular, the density map at cross-sectional cuts exhibits hollow images, indicating that the carbon atoms are systematically deposited along the zeolite supercage surface. However, in the narrow space between adjoining supercages, the electron densities are more diffuse and crowded. Some of the density portions are too close to assign carbon–carbon bonding. This can be interpreted as the average electron-density map superimposing various atomic positions over many identical pore necks—in other words, there is high static disorder. Because of the severe disorder and fractional occupancy, the exact single-crystal structure was difficult to solve unless constraints were used in the refinement process (Extended Data Table 1, Extended Data Fig. 4, and Methods).

The carbon framework obtained at 600 °C can be separated from the template, by using a mixture of hydrogen fluoride and hydrochloric acid to remove the zeolite. The carbon thus recovered exhibits a narrow distribution of pore diameters in the micropore region, corresponding to the thickness of the template walls. The carbon, however, exhibits only poorly resolved XRD peaks and transmission electron microscope (TEM) lattice fringes, indicating that the pores are not well ordered. The loss of pore order seems to result from insufficient formation of carbon–carbon bonds in the narrow necks between adjacent supercages at 600 °C. To obtain a carbon product with highly ordered pores, the carbon–zeolite composite needs to be heated to 850 °C after the carbon-deposition step at 600 °C. This heat treatment involves a small lattice contraction of the zeolite and loss of more than half of the XRD peaks (Supplementary Fig. 1), indicating that the zeolite template behaves like a shrinking mould to allow a rigid carbon framework to form.

The final carbon product—which is liberated from LaY after heating at 850 °C—is an exact replica of the zeolite pore structure. This carbon exhibits highly (for a microporous carbon) well ordered structures in TEM images and powder XRD patterns (Fig. 2 and Supplementary Fig. 2). The TEM images show no carbon deposition on external surfaces. Approximately 80% of the zeolite pores are replicated with carbon (see Supplementary Discussion and Supplementary Fig. 3 for a more detailed quantitative analysis of the 'quality' of carbon replication). This carbon exhibits high thermal stability in air, as compared with mesoporous carbons that are composed of amorphous frameworks[24], or with other zeolite-templated carbons that are synthesized by two-step carbon infiltration into H$^+$ or Na$^+$ zeolites (Extended Data Fig. 5). The thermal stability of the carbon is comparable to that of graphene nanosheets. The high thermal stability and well ordered structure can be attributed to nothing but the effect of lanthanum on carbon deposition. To check this effect, we carried out La^{3+}-ion-exchange into EMT and beta zeolites, and used these zeolites as templates. The resulting carbon frameworks also exhibit high thermal stability and a highly ordered microporous structure (Fig. 2, Supplementary Fig. 2 and Extended Data Fig. 5).

We investigated the possibility of observing a graphene-like atomic arrangement by means of a high-resolution TEM instrument (see Methods), but we failed to obtain direct atomic images. The carbon framework was instantly damaged under the atomic-scale observation condition (which requires an electron beam of very high intensity), even when the electron-acceleration voltage was reduced to 80 kV. In an alternative attempt, we took a selected-area electron-diffraction (SAED) pattern of the carbon synthesized using LaY (Fig. 2e). The SAED pattern showed two low-intensity diffraction rings at the same Bragg angles as graphene (100) and (110) reflections[25], unlike the SAED pattern of amorphous carbon. We interpret the SAED pattern of the LaY-templated carbon as revealing random orientations of six-membered carbon rings existing in a curved, single-layer graphene-like structure. This sp^2 carbon character is confirmed by the NMR spectrum (Extended Data Fig. 3). Moreover, a Raman spectrum shows a strong G-band in addition to a D-band (Extended Data Fig. 6), much like in previous reports on curved nanographene samples[9,26]. The G-band is upshifted from the position of graphite; such a shift is often attributed to a curvature in the graphene structure[9,26]. Another notable feature of the LaY-templated carbon is high electrical conductivity (Fig. 2f and Extended Data Fig. 7). We investigated local electrical conductance using conductive probe atomic force microscopy. The result indicates that electrical conductivity of the LaY-templated carbon is two orders of magnitudes higher than that of the mesoporous carbon CMK-3, which has an amorphous framework[24].

Given these results, we tested the possibility of using other metal ions for ion exchange. We chose Y^{3+} and Ca^{2+}, because these metal

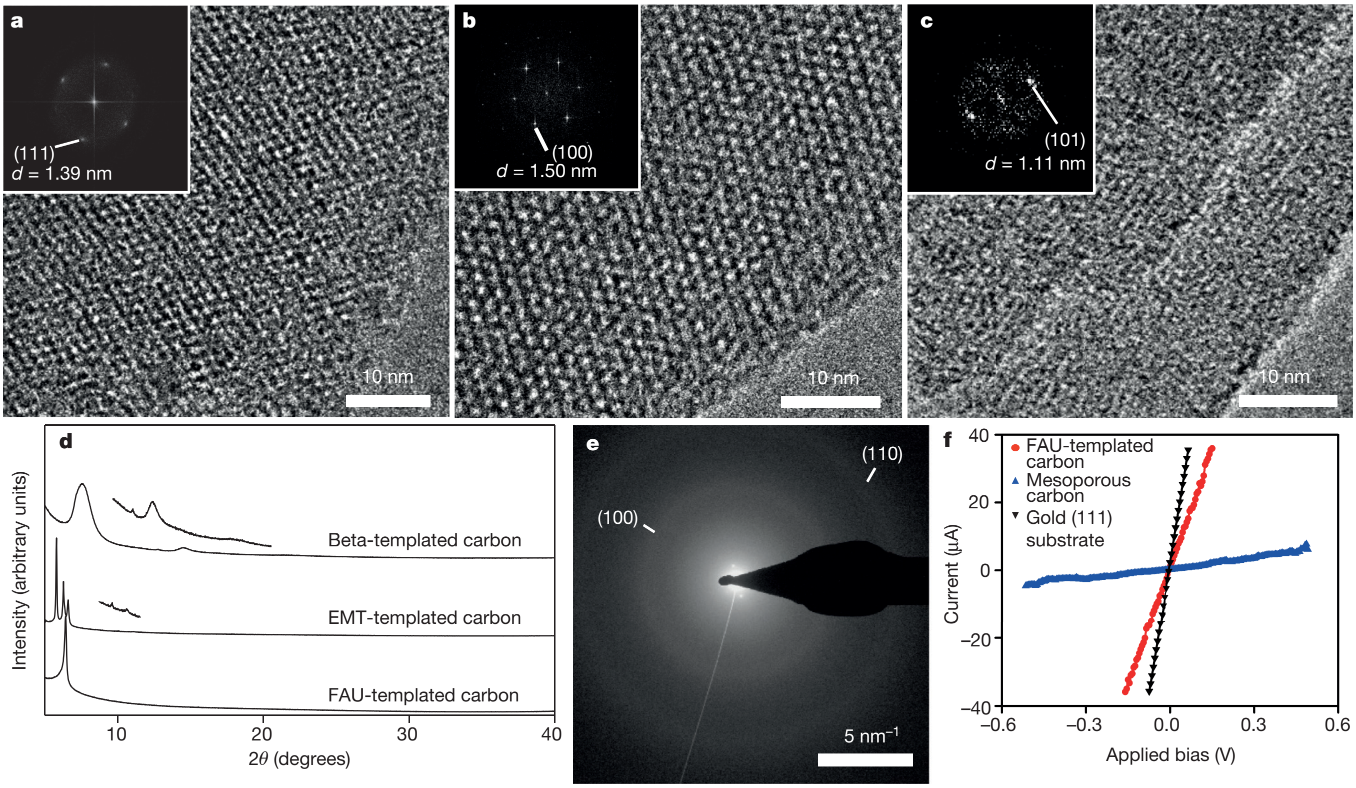

Figure 2 | Structures of 3D graphene-like microporous carbons. **a–c**, TEM images (main pictures) and Fourier diffractograms (insets) of template-free carbon, generated using a template of La^{3+}-ion-exchanged FAU (**a**), EMT (**b**) or beta (**c**) zeolites. The images reveal an ordered pore structure without any external carbon. **d**, Powder XRD patterns from the carbon samples, measured using synchrotron radiation. The patterns reveal the highly ordered microporous structure of the carbons, corresponding to the pore structure of the template. **e**, Electron-diffraction pattern of a selected area from the FAU-templated carbon, showing low-intensity rings corresponding to graphene (100) and (110) reflections. **f**, Current–voltage curves for FAU-templated carbon and CMK-3 mesoporous carbon on a gold (111) substrate, measured by conductive probe atomic force microscopy.

ions are known to interact via coordination bonding with the carbon framework, using electron-donation/back-donation mechanisms[27,28] in a similar way to La^{3+}. Indeed, the exchange of Y^{3+} or Ca^{2+} with ions in FAU-Y dramatically increases the rate of carbon deposition at 600 °C, much as does the LaY zeolite (Supplementary Fig. 4). The final carbon products from these zeolite templates exhibit highly ordered microporous structures. Another critical factor affecting carbon deposition is that water vapour should be fed into the ethylene gas stream. Without water vapour, none of the La^{3+}-, Y^{3+}- and Ca^{2+}-ion-exchanged zeolites shows sufficient carbon deposition. We speculate that this phenomenon could be related to the production of carbides, which the three metal elements used here can form. Typical carbide formation in the bulk state requires high-temperature treatments in an electric arc furnace. However, when metal ions are atomically dispersed in a zeolite framework, a carbide might form even at 600 °C. If so, then as the carbide reacts with water vapour, active carbonaceous species might be generated to construct carbon frameworks.

Acetylene gas can be used instead of ethylene to construct carbon frameworks on the ion-exchanged zeolites. Because acetylene is more reactive than ethylene, carbon deposition can be accomplished at temperatures as low as 340 °C (Supplementary Fig. 5). In addition, the smaller molecular size of acetylene enables uniform infiltration of carbon—even in zeolites with one-dimensional channels (for example, LTL zeolite) or small pore mouths (LTA and MFI zeolites), which have been difficult to use as carbon templates[12,13] (Fig. 3). The LTL zeolite has a one-dimensional (1D) undulating channel, with narrow sections of diameter 0.71 nm and wide sections of diameter 1.24 nm, which alternate with a 0.48-nm periodicity. Accordingly, undulating carbon tubes can be synthesized inside the La^{3+}-exchanged LTL zeolite. When the template walls are removed after heating at 850 °C, the carbon tubes self-assemble to form a bundle (Fig. 3a, b). In contrast, if we use the Na^{+} or H^{+} form of LTL zeolite, carbon deposition occurs only at the external surfaces of the template (Extended Data Fig. 8).

Meanwhile, in the Ca^{2+}-exchanged LTA zeolite, the pore diameter is 1.14 nm; the pores are interconnected to a 3D network, but the pore mouths (of diameter 0.5 nm) are too narrow to have previously considered using LTA as a carbon template. Nonetheless, our results show that carbon infiltrates quite uniformly throughout the entire volume of this zeolite. The final carbon product, liberated from the template, exhibits the crystal morphology of the zeolite template (Fig. 3c), and lattice fringes (Fig. 3e). The carbon crystal can be easily crushed by hand rubbing. The crushed crystal surfaces indicate that the entire volume of the zeolite crystal is used for carbon synthesis (Fig. 3d). Notably, the carbons obtained from the LTL and LTA zeolites can be dispersed in *N*-methylpyrrolidone (NMP); the solutions show photoluminescence, indicating that they are soluble in organic solvents (Fig. 3f). Moreover, the LTA-templated carbon recrystallizes when isopropyl alcohol is added to the NMP solution, indicating that the carbon products show van der Waals packing of carbon nanotubes or carbon dots.

Compared with the LTL and LTA zeolites, the MFI zeolite is somewhat more difficult to use to accomplish carbon synthesis. This is because this zeolite has only narrow channels (<0.56 nm in diameter), without bulged sections. The channels are too narrow to accommodate even C_{60} fullerene. Nevertheless, our results show that these narrow pores can still be used as a template for a carbon nanostructure, and that the morphology of the resulting carbons closely resembles that of the template. The carbon exhibited a sharp peak centred at 0.49 nm in the pore size distribution (Supplementary Fig. 6). This corresponds to

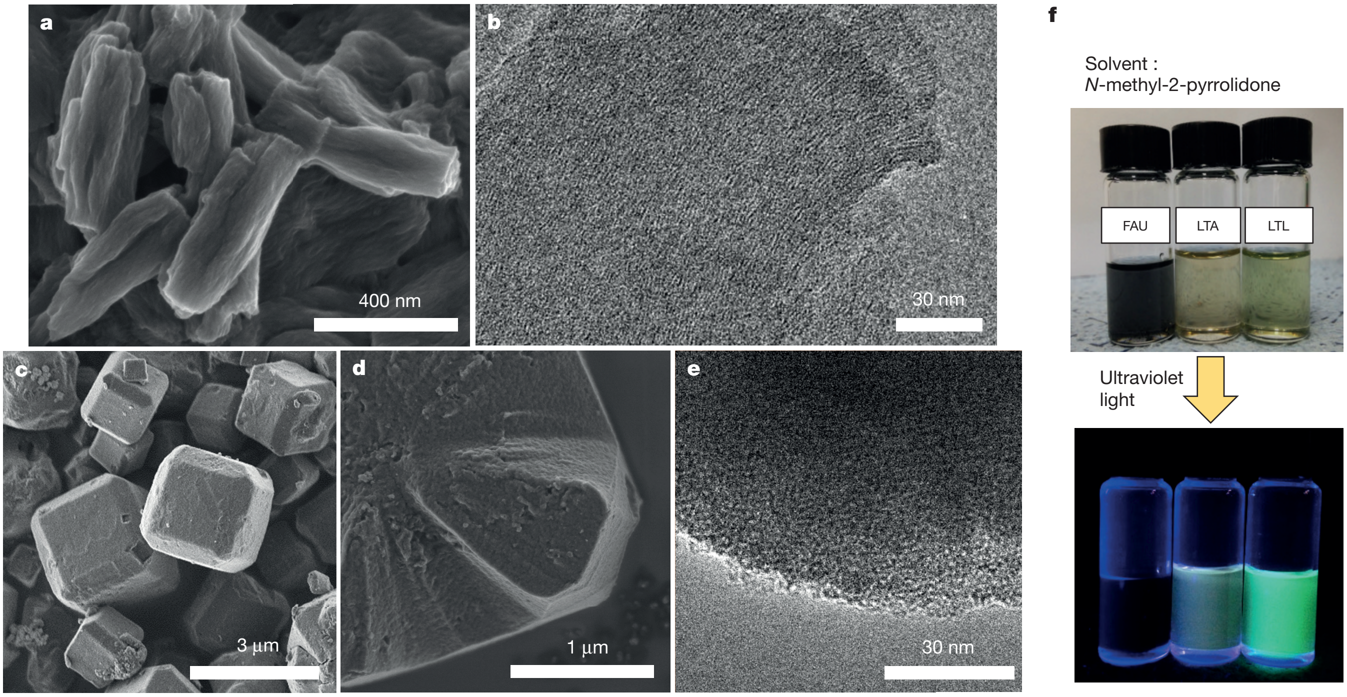

Figure 3 | Carbon from a 1D-channel LTL zeolite, and from a small-pore LTA zeolite. a, Scanning electron microscope (SEM) and **b**, TEM images of LTL-templated carbon, revealing morphologies corresponding to a bundle of 1D channels. **c**, **d**, SEM and **e**, TEM images of LTA-templated carbon, exhibiting zeolite-like crystal morphologies and pore order; these soft carbon crystals can be easily crushed. The SEM image of the broken crystal surfaces (**d**) shows that carbon synthesis uses the entire volume of the zeolite crystal. **f**, Photographs of the LTA- and LTL-templated carbons dispersed in NMP solution, in comparison with FAU. The carbon products from the LTA and LTL templates are soluble and exhibit photoluminescence under ultraviolet light, but the carbon from the FAU template is insoluble. In the latter case, the carbon is synthesized in the form of a 3D porous network that extends over several supercages, rendering it insoluble in organic solvents. However, in the case of the LTA and LTL zeolites, the carbon is obtained as quantum dots or nanotubes; these small carbon objects, which are like fullerenes and carbon nanotubes, are soluble in organic solvents.

the thickness of the MFI pore walls, indicating the formation of rigid carbon nanostructures inside the narrow zeolite channel.

Making graphene with 3D periodic nanoporous architectures promises a range of useful applications, such as in batteries and catalysts[29,30], but has not yet seen full success owing to the lack of efficient synthetic strategies. Our protocol, with its pore-selective carbon filling at decreased temperatures, can be readily scaled up for studies requiring bulk quantities of carbon (Extended Data Fig. 9). Moreover, the high electrical conductivity of the resulting carbon frameworks will be useful in battery applications (Supplementary Fig. 7).

Online Content Methods, along with any additional Extended Data display items and Source Data, are available in the online version of the paper; references unique to these sections appear only in the online paper.

Received 22 October 2015; accepted 20 April 2016.
Published online 29 June 2016.

1. Han, S., Wu, D., Li, S., Zhang, F. & Feng, X. Porous graphene materials for advanced electrochemical energy storage and conversion devices. *Adv. Funct. Mater.* **26,** 849–864 (2014).
2. Jiang, L. & Fan, Z. Design of advanced porous graphene materials: from graphene nanomesh to 3D architectures. *Nanoscale* **6,** 1922–1945 (2014).
3. Cao, X., Yin, Z. & Zhang, H. Three-dimensional graphene materials: preparation, structures and application in supercapacitors. *Energy Environ. Sci.* **7,** 1850–1865 (2014).
4. Vanderbilt, D. & Tersoff, J. Negative-curvature fullerene analog of C_{60}. *Phys. Rev. Lett.* **68,** 511–513 (1992).
5. Mackay, A. L. & Terrones, H. Diamond from graphite. *Nature* **352,** 762 (1991).
6. Lenosky, T., Gonze, X., Teter, M. & Elser, V. Energetics of negatively curved graphitic carbon. *Nature* **355,** 333–335 (1992).
7. Ma, Z., Kyotani, T. & Tomita, A. Preparation of a high surface area microporous carbon having the structural regularity of Y zeolite. *Chem. Commun.* **23,** 2365–2366 (2000).
8. Ma, Z., Kyotani, T., Liu, Z., Terasaki, O. & Tomita, A. Very high surface area microporous carbon with a three-dimensional nano-array structure: synthesis and its molecular structure. *Chem. Mater.* **13,** 4413–4415 (2001).
9. Nishihara, H. *et al.* A possible buckybowl-like structure of zeolite templated carbon. *Carbon* **47,** 1220–1230 (2009).
10. Nueangnoraj, K. *et al.* Formation of crosslinked-fullerene-like framework as negative replica of zeolite Y. *Carbon* **62,** 455–464 (2013).
11. Parmentier, J., Gaslain, F. O. M., Ersen, O., Centeno, T. A. & Solovyov, L. A. Structure and sorption properties of a zeolite-templated carbon with the EMT structure type. *Langmuir* **30,** 297–307 (2014).
12. Kyotani, T., Ma, Z. & Tomita, A. Template synthesis of novel porous carbons using various types of zeolites. *Carbon* **41,** 1451–1459 (2003).
13. Yang, Z., Xia, Y. & Mokaya, R. Enhanced hydrogen storage capacity of high surface area zeolite-like carbon materials. *J. Am. Chem. Soc.* **129,** 1673–1679 (2007).
14. Yang, Z., Xia, Y., Sun, X. & Mokaya, R. Preparation and hydrogen storage properties of zeolite-templated carbon materials nanocast via chemical vapor deposition: effect of the zeolite template and nitrogen doping. *J. Phys. Chem. B* **110,** 18424–18431 (2006).
15. Zhou, J. *et al.* Effect of cation nature of zeolite on carbon replicas and their electrochemical capacitance. *Electrochim. Acta* **89,** 763–770 (2013).
16. Corma, A. From microporous to mesoporous molecular sieve materials and their use in catalysis. *Chem. Rev.* **97,** 2373–2420 (1997).
17. Davis, M. E. & Lobo, R. F. Zeolite and molecular sieve synthesis. *Chem. Mater.* **4,** 756–768 (1992).
18. Davis, M. E. Ordered porous materials for emerging applications. *Nature* **417,** 813–821 (2002).
19. Corma, A. State of the art and future challenges of zeolites as catalysts. *J. Catal.* **216,** 298–312 (2003).
20. Kyotani, T., Nagai, T., Inoue, S. & Tomita, A. Formation of new type of porous carbon by carbonization in zeolite nanochannels. *Chem. Mater.* **9,** 609–615 (1997).
21. Johnson, S. A., Brigham, E. S., Ollivier, P. J. & Mallouk, T. E. Effect of micropore topology on the structure and properties of zeolite polymer replicas. *Chem. Mater.* **9,** 2448–2458 (1997).
22. Guisnet, M. & Magnoux, P. Organic chemistry of coke formation. *Appl. Catal. A Gen.* **212,** 83–96 (2001).
23. Deschamps, M. *et al.* Exploring electrolyte organization in supercapacitor electrodes with solid-state NMR. *Nature Mater.* **12,** 351–358 (2013).
24. Jun, S. *et al.* Synthesis of new, nanoporous carbon with hexagonally ordered mesostructured. *J. Am. Chem. Soc.* **122,** 10712–10713 (2000).
25. Liu, X., Giordano, C. & Antonietti, M. A facile molten-salt route to graphene synthesis. *Small* **10,** 193–200 (2014).
26. Ning, G. *et al.* Gram-scale synthesis of nanomesh graphene with high surface area and its application in supercapacitor electrodes. *Chem. Commun.* **47,** 5976–5978 (2011).

27. Chakraborty, B., Modak, P. & Banerjee, S. Hydrogen storage in yttrium-decorated single walled carbon nanotube. *J. Phys. Chem.* **116,** 22502–22508 (2012).
28. Yoon, M. *et al.* Calcium as the superior coating metal in functionalization of carbon fullerenes for high-capacity hydrogen storage. *Phys. Rev. Lett.* **100,** 206806 (2008).
29. Odkhuu, D. *et al.* Negatively curved carbon as the anode for lithium ion batteries. *Carbon* **66,** 39–47 (2014).
30. Zhai, Y., Zhu, Z. & Dong, S. Carbon-based nanostructures for advanced catalysis. *ChemCatChem* **7,** 2806–2815 (2015).

Supplementary Information is available in the online version of the paper.

Acknowledgements This work was supported by IBS-R004-D1. The authors thank D. Ahn at the Pohang Accelerator Laboratory (PLS) for discussions on powder XRD measurements. X-ray crystallography was carried out with help from D. Moon at PLS and H. J. Lee at Korea Basic Science Institute.

Author Contributions R.R. selected metal-ion catalysts intuitively, initiated single-crystal investigation, and led the project. K.K. led the synthesis and characterization work, with T.L. and Y.K. Y.S. carried out NMR measurements. J.S. and J.K.P. carried out electrochemical analysis. H.L. and J.Y.P. analysed the electrical conductivity of the carbon product. S.J.C. and T.L. carried out the X-ray crystallography. H.I. investigated the mechanism of carbon formation. R.R. and K.K. wrote the manuscript.

Author Information Reprints and permissions information is available at www.nature.com/reprints. The authors declare no competing financial interests. Readers are welcome to comment on the online version of the paper. Correspondence and requests for materials should be addressed to R.R. (rryoo@kaist.ac.kr).

Reviewer Information *Nature* thanks P. de Jongh, L. Solovyov and the other anonymous reviewer(s) for their contribution to the peer review of this work.

METHODS

Preparation of zeolite templates. Zeolite beta (Si/Al ratio = 12.5) was purchased from Zeochem, and MFI (Si/Al = 11.5) from Zeolyst. Other zeolites were synthesized according to literature procedures[31,32]. For X-ray crystallography, we synthesized zeolite FAU with large single-crystal morphology[33]. Ion exchange was performed with aqueous solution of metal salts.

Synthesis of carbon materials. Zeolite was heated to 600 °C under a dry N_2 flow, using a vertically placed, fused quartz reactor equipped with a fritted disk. We passed a mixture of ethylene gas, N_2 and steam through the zeolite bed at 600 °C. The gas flow was switched to dry N_2 when carbon deposition was completed. Then, we increased the temperature to 850 °C, and maintained it there for 2 hours. The resulting product was slurried in a 0.3 M HF/0.15 M HCl solution, or alternatively in concentrated HCl followed by hot 2 M NaOH solution, to release carbon from template. The HF-etched carbon products exhibited an oxygen/carbon ratio of 0.009 in molar ratio, while the carbon samples obtained with NaOH washing had an oxygen/carbon ratio of 0.10.

Collection of crystallographic data. A single crystal (about 35 μm in diameter; see Supplementary Fig. 8) of La FAU zeolite containing carbons, treated at 600 °C, was dehydrated by flowing high-purity N_2 gas at 600 °C for 2 hours, and then put under vacuum at 350 °C for 2 hours, to fully exclude moisture. A crystal was coated with a layer of Paratone oil (pre-dehydrated for 48 hours) in a glove box, in order to prevent moisture absorption during sample mounting and XRD measurements (see Supplementary Fig. 9 for experimental verification through a gravimetric measurement). The coated crystal was measured at 123 K over the range of $2\theta = 5°–149°$, using a Bruker D8-Venture diffractometer with graphite-monochromated CuKα radiation ($\lambda = 0.15418$ nm) and a Photon 100 CMOS detector, at the Korea Basic Science Institute (exposure time = 120 seconds per frame). The Bruker APEX2 program was used for data collection, and SAINT was used for cell refinement and reduction[34]. Absorption correction was applied using the SADABS program[35].

Derivation of electron-density maps for carbon. XRD data, collected from the zeolite–carbon composite crystal, were analysed by means of full-matrix least-squares calculations based on F^2 values with JANA2006 (ref. 36). We found the data to have an $R_{\rm int}$ (observed/all) value of 4.73/5.61 for 547/819 reflections, averaged from 3,996/7,829 reflections, with a redundancy and completeness of 9.559 and 99.9%, respectively. $R_{\rm int}$, the merging error, is given by $R_{\rm int} = \frac{\sum|F_0^2 - F_0^2(\text{mean})|}{\sum F_0^2}$, where F_0 is the experimental structure factor. We obtained an electron-density map by using a dual space method with a charge flipping algorithm[37]. We obtained the space group of $Fd\bar{3}m$, with an overall agreement factor of 2.85, from the electron-density map[38]. We discovered a total of eight atoms in an asymmetric unit, all in the zeolite framework. Refinement of the zeolite framework structure was started after assigning correct atom species using the full-matrix least-squares procedure. The value of maximum (change/s.u.), which is used as a convergence criterion, decreased from 0.05 to 0.01 during this initial refinement process (s.u. is the standard uncertainty). The values of R_1/wR_2 (which indicate the agreement between the crystallographic model and the experimental X-ray diffraction data) were 18.73/43.00 when Si and O atoms were taken into account for the framework.

For further refinement, including La and Na atoms, first, the scale factor of the zeolite crystal containing carbons was determined using the high-angle portion above $\sin\theta/\lambda = 0.25$ corresponding to $d \leq 0.2$ nm[39] (where d indicates the resolution, defined by the Breck equation, $\lambda = 2d\sin\theta$ This process yielded R_1/wR_2 values of 9.74/21.04 for 747 unique reflections. The R_1/wR_2 values decreased to 7.49/15.81 when occupancy factors for non-framework species (that is, Na, La, and O atoms bound to La) were refined. Second, anisotropic atomic displacement factors were used for all zeolite framework atoms and La atoms. Isotropic atomic displacement factors were used for non-framework atoms except La. This process further decreased R_1/wR_2 to 6.30/12.78. The resulting composition of the zeolite was $|\mathrm{La}_{23.32}\mathrm{Na}_{12.16}\mathrm{O}_{12.12}|[\mathrm{T(Si,Al)O_2}]_{192}$, which was consistent with that from the chemical analysis.

In this stage, we tried to refine intrapore species using all reflections including the low-angle portion (that is, 819 unique reflections). The scale factor, determined above, was fixed until most of the missing intrapore atoms were assigned from a difference Fourier method. In a first trial of the difference Fourier method, we found eight peaks. Two peaks were assigned as oxygen that was coordinated to La in the zeolite framework, and six peaks were assigned as carbon in the zeolite pore space. The refinement of occupancy factors and positions of the obtained eight missing peaks resulted in R_1/wR_2 decreasing to 7.07/17.91. The thermal displacement factor for all carbon atoms was set to a reasonable value, $U_{\rm iso} = 0.08$ Å^2, according to ref. 40. By using the difference Fourier method again, we also found three carbon atoms. Refinement of the additional carbon and oxygen yielded R_1/wR_2 values of 6.66/15.72. Further inclusion of carbon atoms using the difference Fourier method did not improve the R factors. Thus, by this stage, it could be considered that most of the missing atoms were found. The obtained composition was $|\mathrm{C}_{207.58}\mathrm{La}_{23.52}\mathrm{Na}_{14.27}\mathrm{O}_{26.69}|$ $[\mathrm{T(Si,Al)O_2}]_{192}$. The carbon content is comparable to the empirical carbon content (258 atoms per unit cell) obtained from elemental analysis of the sample. The obtained composition was changed slightly by the subsequent additional refinement of the structural parameters with the scale factor.

In the last refinement, the occupancy factor of carbon atoms was fixed, and all carbon atoms were assumed to have the same atomic displacement parameter. The constraints listed in a CIF file (see Supplementary information) were automatically generated from the symmetry operation, based on this assumption. Refinement using these constraints was continued until R_1/wR_2 values reached 5.40/13.65 with 547 reflections for $I > 3\sigma(I)$ (where I is the reflection intensity). The largest difference peak was 0.50, and the deepest hole was −0.43 e Å^{-3}. The goodness-of-fitness index was 1.9. The final maximum (change/s.u.) was 0.0051. However, when all 819 reflections were taken into account, the R_1/wR_2 values were 7.89/14.36. Moreover, attempts to refine each carbon atomic displacement parameter independently, without using constraints, failed to give stable convergence. In this regard, the above refinement result using constraints may not yet provide an accurate structural solution. After removing the carbon atoms obtained from structure refinement with constraints, we visualized an electron-density map corresponding to the carbon structure using the difference Fourier method; this map was equivalent to the difference between the total electron-density map and an electron-density map that corresponds to the zeolite framework.

Characterization. We determined the carbon content in zeolites by thermogravimetry using a TGA Q50 (TA Instruments). We collected powder XRD data using a monochromated synchrotron X-ray at Beamline 9B of the Pohang Accelerator Laboratory. TEM images and SAED patterns were collected with a Titan E-TEM G2 (FEI) at 300 kV acceleration voltages, on a holey carbon grid (300 mesh) after supporting with ethanol dispersion. SEM images were taken with a Verios 460 (FEI) at a landing voltage of 1 kV in deceleration mode (stage bias voltage: 5 kV). ^{13}C NMR spectra were acquired with magic-angle spinning using Brucker Avance III HD 400WB. Raman spectra were recorded on a Horiba Jobin Yvon ARAMIS spectrometer with a laser excitation wavelength of 514 nm. Electrical conductance was measured using an Agilent atomic force microscope 5500 in air, with a Pt/Ir-coated tip (PPP-EFM-50, Nanosensors).

31. Breck, D. W. *Zeolite Molecular Sieves* (Wiley, 1974).
32. Delprato, F., Delmotte, L., Guth, J. L. & Huve, L. Synthesis of new silica-rich cubic and hexagonal faujasites using crown-ether-based supramolecules as templates. *Zeolites* **10,** 546–552 (1990).
33. Ferchiche, S., Warzywoda, J. & Sacco, A., Jr Direct synthesis of zeolite Y with large particle size. *Int. J. Inorg. Mater.* **3,** 773–780 (2001).
34. APEX2 and SAINT (Bruker AXS, 2014).
35. Sheldrick, G. M. *SADABS* (Univ. Göttingen, 2008).
36. Petříček, V., Dušek, M. & Palatinus, L. Crystallographic computing system JANA2006: general features. *Z. Kristallogr.* **229,** 345–352 (2014).
37. Palatinus, L. & Chapuis, G. SUPERFLIP—a computer program for the solution of crystal structures by charge flipping in arbitraray dimensions. *J. Appl. Cryst.* **40,** 786–790 (2007).
38. Palatinus, L. & van der Lee, A. Symmetry determination following structure solution in *P*1. *J. Appl. Cryst.* **41,** 975–984 (2008).
39. McCusker, L. B., Von Dreele, R. B. & Cox, D. E., Louër, D. & Scardi, P. Rietveld refinement guidelines. *J. Appl. Cryst.* **32,** 36–50 (1999).
40. Xie, D., McCusker, L. B. & Baerlocher, C. Structure of the borosilicate zeolite catalyst SSZ-82 solved using 2D-XPD charge flipping. *J. Am. Chem. Soc.* **133,** 20604–20610 (2011).
41. Biener, J. *et al.* Macroscopic 3D nanographene with dynamically tunable bulk properties. *Adv. Mater.* **24,** 5083–5087 (2012).

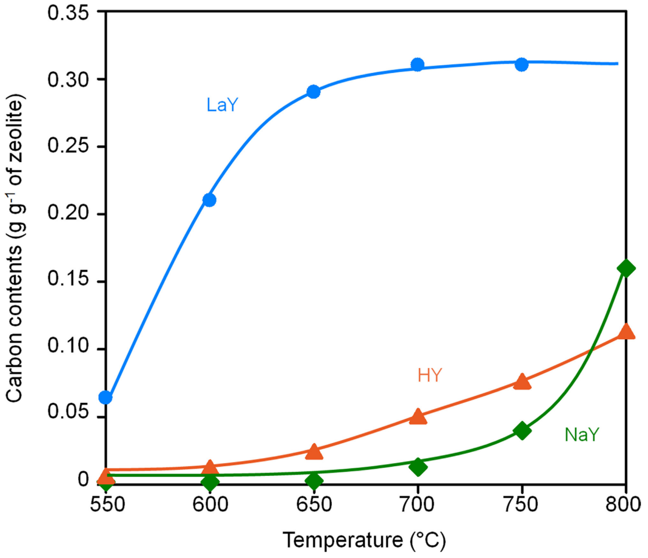

Extended Data Figure 1 | Carbon deposition in zeolite FAU plotted as a function of temperature, with various ion exchanges. The zeolites LaY, NaY and HY were heated to the temperatures indicated under a dry N_2 flow, using a vertically placed, fused quartz reactor equipped with a fritted disk. Subsequently, a mixture of ethylene gas, N_2 and steam was passed through the zeolite bed for 1 hour. The amount of carbon deposited at each temperature was measured by thermogravimetry. At 600 °C, the La^{3+}-ion-exchanged zeolite had been deposited with 20 times more carbon than had HY or NaY.

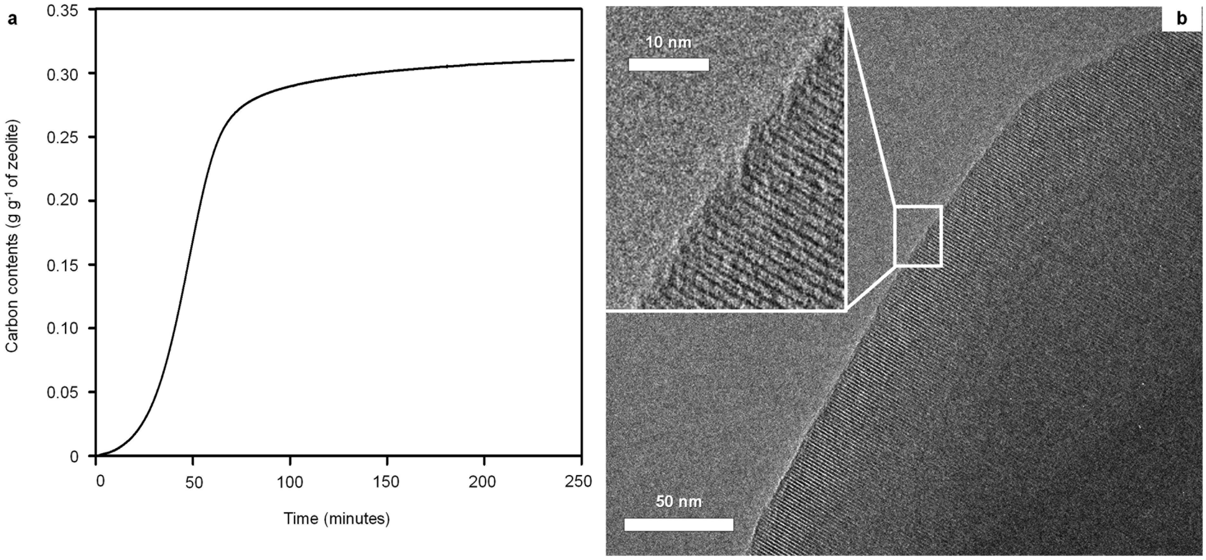

Extended Data Figure 2 | Carbon deposition in La^{3+}-ion-exchanged FAU zeolite at 600 °C. a, The amount of carbon was measured as a function of time, using thermogravimetric analysis equipment built in the carbon deposition rig. The plotted result indicates that the carbon content in LaY becomes saturated at ~0.3 g g^{-1} of zeolite. **b**, A TEM image of LaY zeolite after 250 min of carbon deposition, showing apparently no carbon deposition on external surfaces.

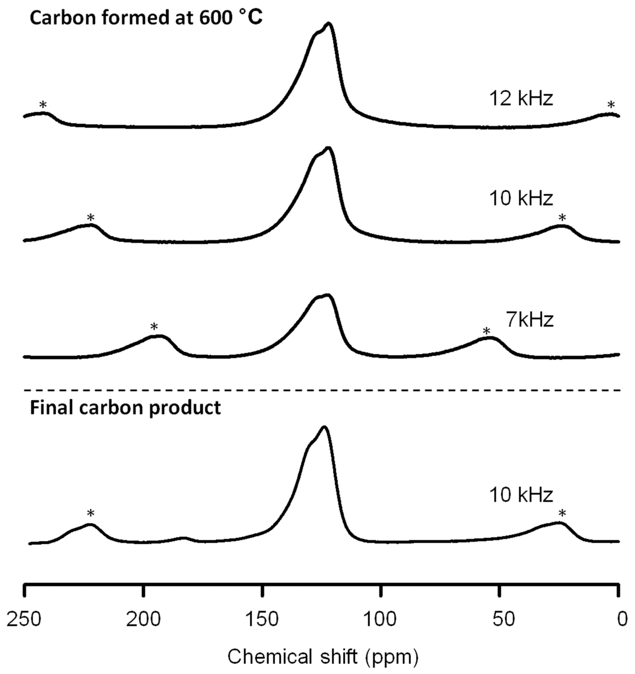

Extended Data Figure 3 | Magic-angle spinning solid-state ^{13}C NMR spectra of the carbon framework formed within zeolite LaY. The NMR spectra were recorded with various spinning rates on a Brucker Avance III HD 400WB NMR spectrometer operated at 100.61 MHz for ^{13}C. All spectra were obtained with a 4-μs pulse, a 10-s relaxation delay, and 1,000 acquisitions. Asterisks indicate spinning sidebands for a given spinning rate. The spectra for carbon obtained at 600 °C exhibit two peaks with chemical shift at 123 p.p.m. and 129 p.p.m. The peak at 123 p.p.m. can be assigned to six-membered-ring sp^2 carbon; the peak at 129 p.p.m. can be attributed to five- or seven-membered rings that have smaller C–C–C angles in the conjugated sp^2 carbon system[24]. No other peaks (assignable to sp^3 or sp carbons) were detected in the NMR spectra of sample prepared with 99% ^{13}C-isotope-enriched ethylene. The final carbon product, liberated from zeolite after heat treatment at 850 °C, has an additional weak peak at around 180 p.p.m., corresponding to oxygen functional groups.

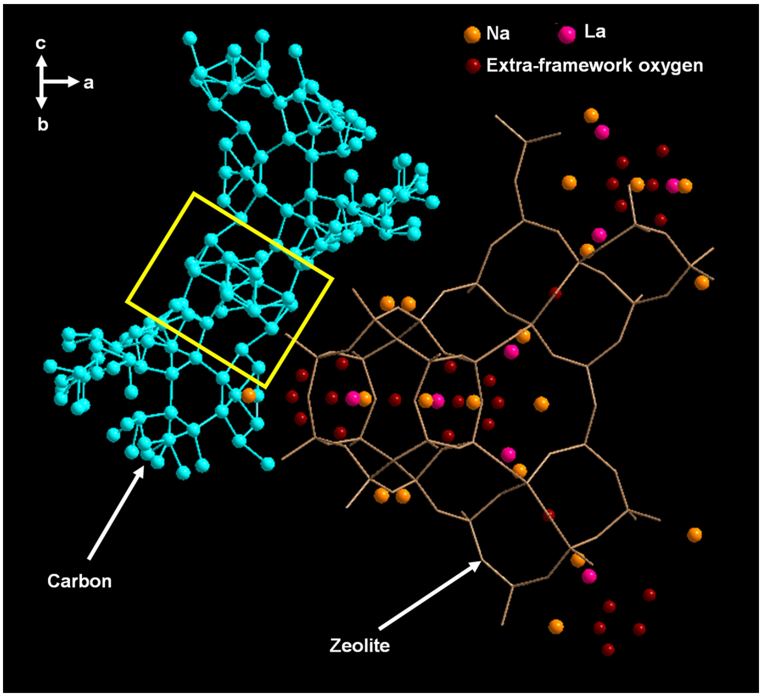

Extended Data Figure 4 | X-ray crystallographic analysis of the carbon structure formed in a single crystal of La^{3+}-ion-exchanged zeolite FAU. Carbon atomic positions were determined through least-square refinement of the distances, using a difference Fourier method (see Methods for details). To cope with a complex system having high static disorder of atomic positions, we assumed that all carbon atoms had the same thermal parameter in the refinement procedure. The refinement result indicates that atomic positions in pore necks (yellow rectangle) have high static disorders over a zeolite crystal. That is, the determined positions can be regarded as overlapped carbon positions over many identical pore necks. This result, using constraints, may not yet provide an accurate structural solution.

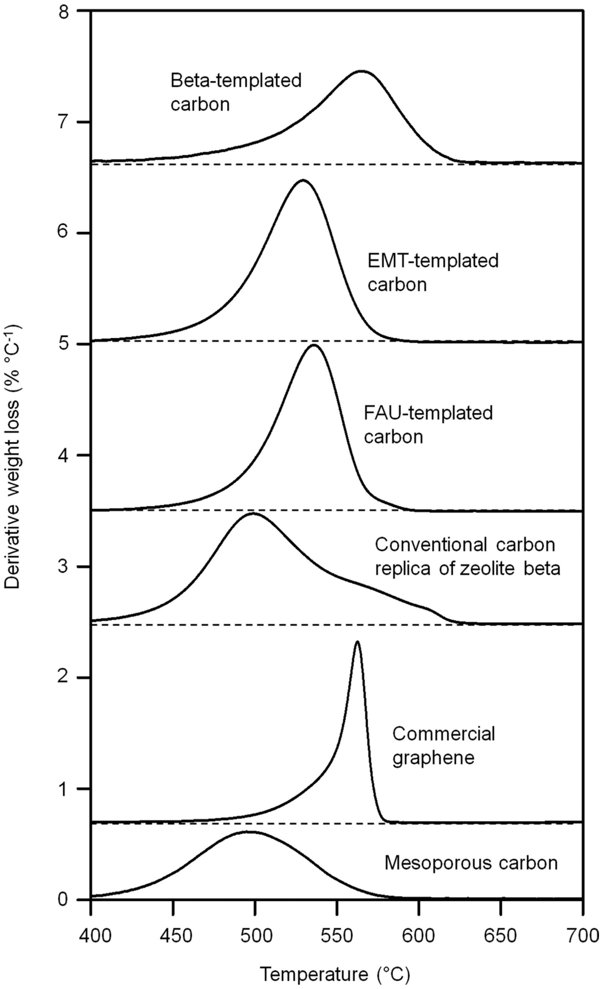

Extended Data Figure 5 | Thermal stability of carbon samples. The top three curves are derivative thermogravimetric curves for the carbons synthesized using different lanthanum-ion-exchanged zeolites. Thermogravimetry was carried out by increasing the temperature to 700 °C, with a ramping rate of 3 °C min^{-1}, under air flow (60 ml min^{-1}). We compared these thermogravimetric data with the results obtained using the mesoporous carbon CMK-3 (which has an amorphous structure), a commercial graphene product (purchased from Graphene Laboratories Inc.), and a beta-zeolite-templated carbon sample that was prepared following a two-step carbonization method[13] (bottom three curves). These data indicate that carbon samples obtained from lanthanum-ion-exchanged zeolites can have distinctively high thermal stability, compared with amorphous carbons. Notably, the beta-templated carbon exhibited high thermal stability in air, like graphene.

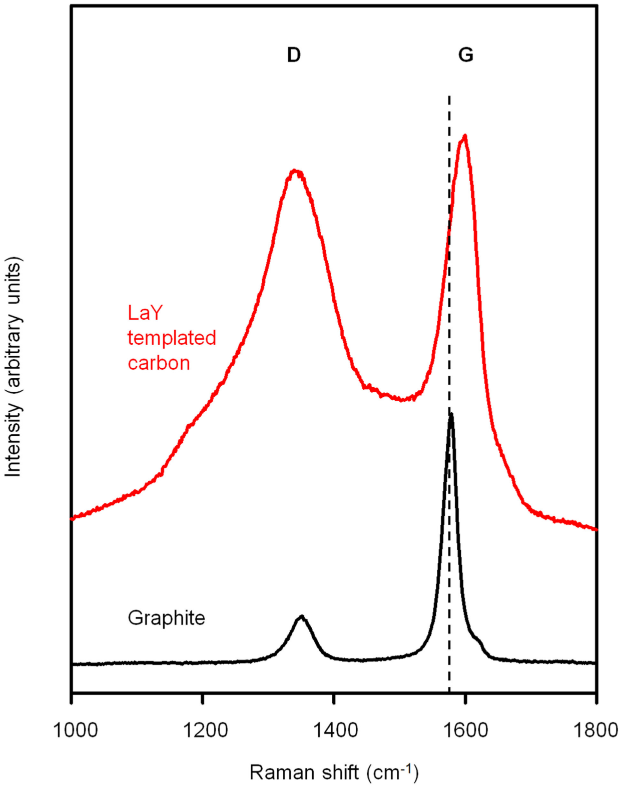

Extended Data Figure 6 | Raman spectra of LaY-templated carbon and graphite. The spectra were recorded on a Horiba Jobin Yvon ARAMIS spectrometer with a laser excitation wavelength of 514 nm. The G- and D-bands are located at 1,598 cm^{-1} and 1,341 cm^{-1}, respectively. The G-band of LaY-templated carbon appears at a higher wavenumber than that of graphite; such a strong upshift indicates nanosized single graphene layers[26]. The broad D-band is attributed to bond disorder, for instance because of the presence of five- or seven-membered carbon rings in the curved carbon structure[41].

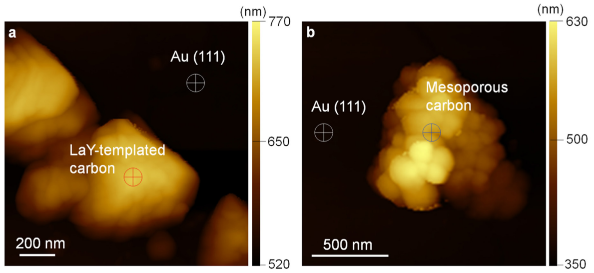

Extended Data Figure 7 | Topographical images of LaY-templated carbon and CMK-3 mesoporous carbon on an Au (111) substrate. **a**, LaY-templated carbon; **b**, CMK-3 mesoporous carbon. The current–voltage curves shown in Fig. 2f were measured on the cross-marked areas. The images were taken using an Agilent 5500 atomic force microscope in air, using a Pt/Ir-coated tip (see Methods).

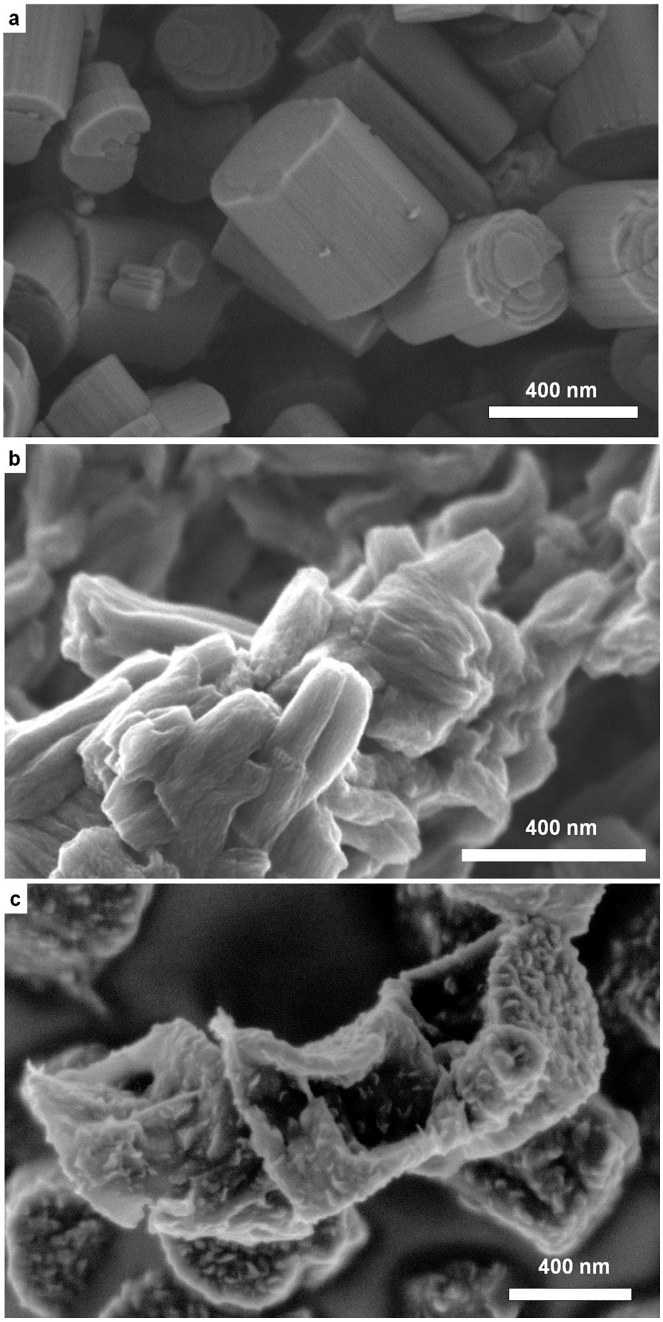

Extended Data Figure 8 | Effect of ion exchange on carbon synthesis using the 1D-channel LTL zeolite. a, SEM image of LTL zeolite. **b**, SEM image of carbon liberated from La^{3+}-ion-exchanged LTL zeolite. **c**, SEM image of carbon from H^{+}-ion-exchanged LTL zeolite. For carbon synthesis using La^{3+}-ion-exchanged zeolite, acetylene gas was used as the carbon source at 500 °C; the remainder of the protocol is as described in the Methods. For the H^{+}-ion-exchanged zeolite, carbon deposition was tested at various temperatures between 500 °C and 700 °C. However, synthesis using this H^{+} zeolite failed.

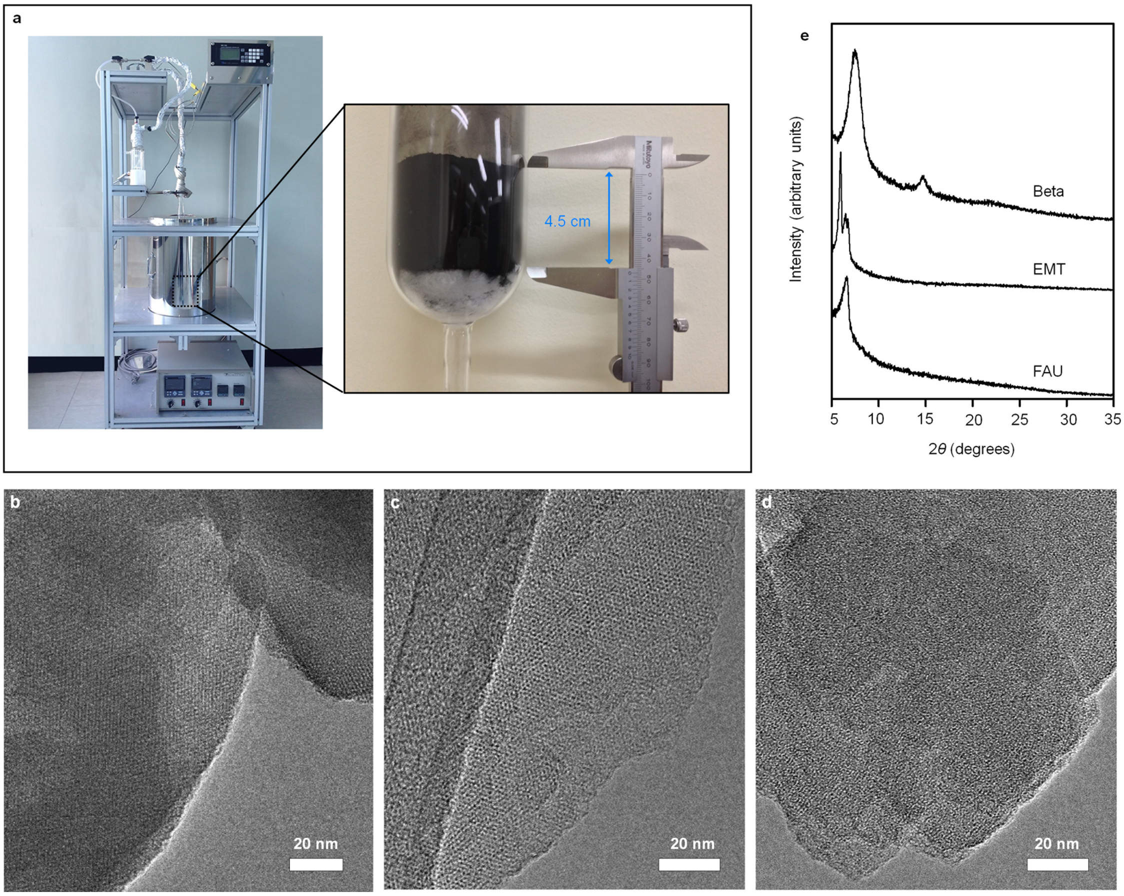

Extended Data Figure 9 | Scaling up the carbon-deposition process. **a**, Photograph of the carbonization rig for large-batch synthesis; inset, the plug-flow reactor filled with a thick bed of carbon–zeolite composite (about 40 g). From this apparatus, we could obtain about 10 g of batch carbon products in a single preparation. **b**–**d**, TEM images of the carbon products synthesized from zeolites FAU (**b**), EMT (**c**) and beta (**d**). **e**, XRD patterns of the carbons, confirming their highly ordered structure. These results indicate that the product quality from the 10-g batch synthesis is the same as that from the 0.15-g batch.

Extended Data Table 1 | Data collection and refinement statistics for X-ray diffraction analysis

Formula	$\|C_{208.03}La_{23.52}Na_{15.50}O_{27.27}\|[T(Si,Al)O_2]_{192}$
Formula weight	18094.3
Temperature	123(2) K
Wavelength	Cu Kα (λ=0.15418 nm)
Crystal system	Cubic
Space group	$Fd\bar{3}m$
Unit cell dimensions	a = 25.0433 Å
Volume	15706.33 $Å^3$
Z	1
Density (calculated)	1.913 Mg/m^3
Absorption coefficient	16.682 mm^{-1}
F(000)	8737
Crystal size	0.035 x 0.035 x 0.035 mm^3
2θ range in data collection	149°
Index range	$-27 \leq h \leq 30$, $-15 \leq k \leq 31$, $-19 \leq l \leq 25$
Reflections collected	7829 [R_{int}(obs/all) = 4.73/5.61]
Completeness to theta = 74.5°	99.9%
Independent reflections (obs/all)	547/819
Refinement method	Full-matrix least-squares on F^2
Data / restraints / parameters	819 / 0 / 71
Goodness-of-fit on F^2	1.90
Final R indices [I>3sigma(I)]	R_1 = 0.0540, wR_2 =0.1365
R indices (all data)	R_1 = 0.0789, wR_2 =0.1436
Largest diff. peak and hole	0.50 and -0.43 $e{\cdot}Å^{-3}$